ACS APPLIED POLYMER MATERIALS

pubs.acs.org/acsapm Article

Polyethylene Blends for Improved Oxygen Barrier: Processing-Dependent Microstructure and Gas Permeability

Kyungtae Kim,* Aristotle J. Zervoudakis, Jacob A. LaNasa, Greg Haugstad, Fang Zhou, Bongjoon Lee, Olivier Lhost, Yves Trolez, Frank S. Bates, and Christopher W. Macosko

Cite This: *ACS Appl. Polym. Mater.* 2024, 6, 524−533 Read Online

ACCESS | Metrics & More | Article Recommendations | Supporting Information

ABSTRACT: This work demonstrates a greater than expected enhancement of oxygen barrier properties in linear low-density polyethylene (LLDPE)-based materials by blending LLDPE with high-density polyethylene (HDPE). The films made by melt pressing the LLDPE/HDPE blends had a greater reduction in oxygen permeability coefficients (P_{O_2}) than predicted using common permeability reduction models, i.e., the harmonic average model and zero-permeability nanofiller model. The reduction of P_{O_2} was attributed to the presence of spherulite crystal structures, as revealed by atomic force microscopy combined with infrared spectroscopy (AFM-IR). The LLDPE matrix exhibited significant spherulite formation even at a relatively low addition of HDPEs, which likely formed tortuous pathways for diffusing oxygen molecules. Transport results from melt-pressed films contrast with the results from films with similar compositions prepared by film blowing, which did not show barrier enhancement beyond expectation. AFM-IR revealed that the blown films lacked spherulite crystals likely due to stretching in the machine direction followed by rapid cooling. These findings demonstrate the role of processing in controlling microstructures and thus the oxygen barrier performance. This work offers the possibility of achieving easily recyclable LLDPE-based packaging materials by simple blending of polyethylenes with different crystalline content.

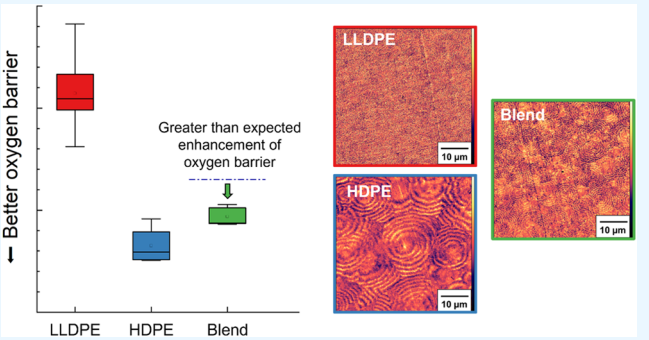

KEYWORDS: *polyethylene packaging, oxygen barrier, polymer blends, blown films, polymer crystallization*

INTRODUCTION

Polyethylene (PE) packaging shares a substantial portion of the US plastic packaging market, valued at USD 112 billion in 2020 and projected to reach USD 148 billion by 2028.[1] Among various grades of PEs, there is an increasing demand for linear low-density PE (LLDPE) films thanks to their high toughness, tear and impact resistance, and high optical transparency compared with other packaging films.[2−4] The nonpolar hydrocarbon chains of LLDPE also endow good moisture barrier properties [i.e., low water vapor transmission rate (WVTR)]. On the other hand, LLDPE films usually suffer a high oxygen transmission rate (OTR), which is detrimental to the packaging of perishable goods (e.g., raw food, cosmetics, and medicine). It is estimated that 20−25% of food waste could be avoided by better packaging design and practices, thereby substantially reducing the environmental impact.[5]

There have been several efforts to improve the gas barrier properties of polymer packaging films.[6−8] To achieve low-OTR PE films, ethylene-vinyl alcohol copolymer (EVOH) is often incorporated as an additional layer or a filler.[8,9] However, EVOH has several drawbacks: it is expensive, brittle, and susceptible to moisture absorption that can lead to a breakdown in oxygen barrier properties, i.e., the film becomes oxygen permeable under high humidity. In addition, since EVOH is chemically distinct from the PE matrix, recycling is not straightforward; in general, EVOH-containing PE resins are recyclable only when the EVOH content is less than 5%.[10] Furthermore, EVOH is mainly incorporated into films as additional layers that necessitate the use of adhesives, which makes recycling EVOH-added films even more difficult. There exist only a few commercial EVOH-containing PE resins that are recyclable (e.g., RecycleReady from the Dow Chemical Company).[11] It is possible to achieve both high oxygen and moisture barrier properties in a single material (e.g., polyvinylidene chloride), but it is desirable to avoid using chlorine-containing polymers due to environmental concerns.[12] There have been other attempts to produce both

Received: September 16, 2023
Revised: November 7, 2023
Accepted: November 17, 2023
Published: December 4, 2023

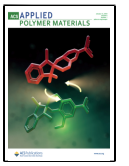

https://doi.org/10.1021/acsapm.3c02211
ACS Appl. Polym. Mater. 2024, 6, 524−533

Table 1. List of Polymers Used in This Study

sample code	commercial name	M_w[a] (kg/mol)	$Đ$[a]	density[b] (g/cm^3)	melt flow index[b] (g/10min@190 °C)
LLDPE1	Total Lumicene M1835	134	2.2	0.918	3.5
LLDPE2	Total Lumicene M2310EP	not measured	not measured	0.923	0.9
HDPE1	Total Lumicene M6040	124	3.3	0.960	4.0
HDPE2	Dow DMDA-8965 NT7	69.0	4.4	0.952	66
HDPE3	Total Lumicene M5510EP	not measured	not measured	0.955	1.2
HDPE4	Total Lumicene M6012EP	not measured	not measured	0.960	1.2
HDPE5	Total 5802	not measured	not measured	0.957	0.3

[a]Measured using HT-SEC. [b]Manufacturer-provided values.

oxygen- and water-resistant PE films by blending PE with low-permeability polymers (e.g., polyethylene terephthalate, polysaccharides)[13−15] and nanofillers (e.g., clay, graphene derivatives),[16−19] but in most cases, the reduction of OTR does not exceed that expected from the volume fraction of the filler materials and WVTR was often compromised when the fillers were hydrophilic, similar to the case of EVOH. Also, such fillers almost always render the film opaque. Moreover, as the filler materials are difficult to separate at the end of use, the problem of recyclability persists. New approaches must be considered to achieve high oxygen barrier films under broad usage conditions that are engineered for sustainability.

This paper reports a greater than expected enhancement of oxygen barrier properties of LLDPE obtained by blending with 10−20 wt % high-density PE (HDPE) with films prepared by melt pressing. Blending 20 wt % HDPE into an LLDPE film reduced the oxygen permeability coefficient (P_{O_2}) of the film by 22−28% more than the values estimated from a theoretical model that describes the reduction of gas permeability by adding nonpermeating nanofillers. This result is compared to mixtures with similar compositions prepared by film blowing, which did not exhibit a barrier enhancement beyond expectation. The oxygen barrier properties of the films made by different processing methods are correlated to the microstructures of the films examined using atomic force microscopy (AFM) equipped with simultaneous infrared (IR) spectroscopy measurement capability. We compare the experimental results with theoretical models developed for impermeable nanofillers. Since both the matrix and filler material are PE, compatibilizers were not required to achieve good dispersion of HDPE in LLDPE. This strategy is also advantageous for recyclability, as the blended films consist only of chemically indistinct PEs.

MATERIALS AND METHODS

Materials and Molecular/Thermal Characterization. All polymer resins, listed in Table 1, were provided in the form of pellets and used as received. All PEs except HDPE2 were provided by TotalEnergies. The Total Lumicene PEs were synthesized using a metallocene catalyst, which resulted in a relatively narrow dispersity ($Đ$) with minimal oligomer content.[20] HDPE2 was provided by the Dow Chemical Company. Weight-average molar mass (M_w) and $Đ$ of the polymers used for melt pressing (i.e., LLDPE1, HDPE1, and HDPE2) were measured using high-temperature size exclusion chromatography (HT-SEC) with 1,2,4-trichlorobenzene as the eluent.[21] Densities and melt flow indices of the materials were provided by the manufacturers. Thermal properties of PE samples were measured using a TA Instruments Q2000 differential scanning calorimeter (DSC) operated at a heating/cooling rate of 2 °C/min.

Preparation of Blends and Blown Films. LLDPE/HDPE blends were prepared using LLDPE1, HDPE1, and HDPE2, through batch mixing for 5 min employing a HAAKE PolyLab OS batch mixer at a rotor speed of 150 rpm and a chamber temperature of 180 °C. Film specimens for P_{O_2} measurements (approximately 100 mm × 100 mm) were melt-pressed using a Carver press with a pressing force of 11,000 N for 2 min at 180 °C. The films were cooled to room temperature by sandwiching them between a pair of precooled metal plates, resulting in final thicknesses of 120−150 μm. Specimens for tensile tests were prepared in a similar manner but with a lower pressing force of 5000 N to achieve final thicknesses of 300−400 μm.

Blown films were produced with mixtures of LLDPE2 and HDPE1, 3, 4, and 5 using a Brabender blown film line. Blends were created by feeding an 80/20 weight ratio of LLDPE2 and HDPE pellets to a 19 mm diameter single screw extruder (length/diameter = 25), maintained at 240 °C and run at 90 rpm, resulting in a total mass flow rate of 1.38 kg/h. The film blowing die had an outer diameter of 50 mm and a die gap of 1 mm and was kept at 235 °C. Upon exiting the die, the film temperature was 225 °C. The blow-up ratio was 2.5, a typical value for this kind of study,[22,23] and the draw rate was adjusted to target a final film thickness of 40 μm.

Oxygen Barrier Property Measurements. OTR of the polymer films was measured following ASTM D3985 (equal pressure method) or D1434 (differential pressure method).[24,25] Melt-pressed and blown films were placed in a measurement cell to partition them into two compartments. Then, according to ASTM D3985, one side was maintained at 1 atm of nitrogen. Air (containing 20.9% oxygen) at 1 atm was maintained on the other side, and the amount of oxygen that passed through the sample film (in cm$^3_{STP}$/day) was measured using an oxygen sensor. This amount of oxygen was divided by the area of the film (in m^2) exposed to air and the partial pressure difference of the oxygen between the two compartments (0.209 atm) to yield the OTR in cm$^3_{STP}$/(m^2·day·atm). When following ASTM D1434, one side of the measurement cell was kept under vacuum while the other side held pure oxygen at 3−25 atm. The amount of oxygen that passed through the film was measured using a vacuum gauge and was divided by the exposed area and the oxygen pressure to yield the ozone-containing concentration (OTR). Finally, the OTR obtained from either method was multiplied by the film thickness to obtain P_{O_2} in cm$^3_{STP}$·mm/(m^2·day·atm), which is the value intrinsic to the material and does not depend on the film thickness.

Film Surface Morphology Investigation Using AFM Combined with IR Spectroscopy (AFM-IR). PE samples were embedded in an epoxy resin and mounted in a Leica UC6 cryomicrotome for AFM-IR sample preparation. The cutting temperature was −140 °C and the cutting speed was 0.4 mm/s, employing a DiATOME cryo AFM diamond knife. Section thickness was ∼300 nm in all cases. Sections were deposited on a clean silicon wafer.

A Bruker NanoIR3 AFM-IR system was operated in the "tapping IR" mode, which is a dual-eigenmode/heterodyne AC implementation as described below. Gold-coated tips attached to silicon cantilevers (Bruker probe type PR-EX-NIR2) were employed. The tip-bearing cantilever was mechanically vibrated at its fundamental flexural resonance. As with conventional AC/tapping mode, upon tip−sample engagement, the setpoint oscillation amplitude was maintained at ∼90% of the free oscillation amplitude during X−Y scanning via Z feedback. At the same time, a MIRcat IR laser (using three QCL chips spanning ca. 900−1800 cm^{-1} wavenumber) was

https://doi.org/10.1021/acsapm.3c02211
ACS Appl. Polym. Mater. 2024, 6, 524−533

pulsed at the difference frequency (f_{pulse} ~ 350 kHz) between the fundamental (f_0 ~ 70 kHz) and the next-higher (f_1 ~ 420 kHz) eigenfrequencies. Sample absorbance at a given wavenumber was sensed when the nonlinear tip−sample interaction (in Z) produced heterodyning between the photothermal expansion (of the sample) pulses that propagated up to the mechanically oscillating tip, whereas excitation occurred at f_1. The amplitude of response at f_1 at a given pixel location quantified the absorbance of IR radiation relative to that at other pixel locations.[26] This response is used to reveal polymer spherulite morphologies, as reported on other polymeric systems.[27] Mechanical driving amplitude and set point were selected to maintain a net attractive interaction, as determined by the net mechanical phase shift at f_0 under tip−sample engagement relative to that in free resonance.[28] This selection allowed stable tip performance from sample to sample over several hours of operation with a given probe.

Common postprocessing of AFM images (plane fitting, etc.) and two-dimensional (2D) Fourier transform (FT) of IR absorbance images were performed using the freeware Gwyddion v2.58. In some cases (see Results and Discussion), the IR absorbance images were divided by height images to renormalize the IR absorbance to the thickness of the microtomed cross sections, given the observation that the IR amplitude sensed by the tip scaled approximately linearly with the thickness of the absorbing sample.

Tensile Property Measurements. A tensile test was performed on melt-pressed samples 24 h after film preparation using a Shimadzu tensile tester operated at a 50 mm/min draw rate. Dog bone-shaped samples with 22 mm gauge length, 5 mm gauge width, and 300−400 μm thicknesses were prepared. Data were averaged over tests on three individual specimens.

RESULTS AND DISCUSSION

HDPE1 and HDPE2, with significantly different molar masses and vastly different melt flow indices (Table 1), were used to investigate how the different grades of HDPEs affect the melt-pressed blend morphology and oxygen barrier properties. The crystallization behavior of the LLDPE1/HDPE blends was examined by using DSC (Figure 1 and Table 2). The blends were named HDPE*j* YY wt %, where *j* = 1 or 2 and YY is the weight percent of the HDPE*j* mixed into the LLDPE1 matrix. The first heating curve shows the thermal history attributed to melt pressing and quenching of the blends. LLDPE and HDPE are semicrystalline, as is evident from the presence of distinct melting peaks. The crystal melting point (T_m) of the HDPEs in the blends decreased by 6−13 °C relative to the pure materials,

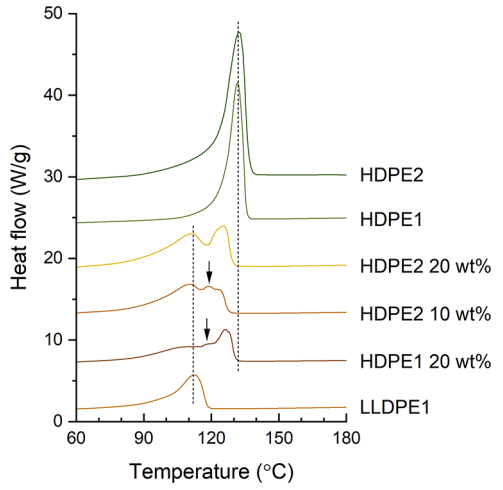

Figure 1. DSC thermograms (first heating) of melt-pressed LLDPE1, HDPE1 and HDPE2, and their blends. The thermal profiles are vertically shifted for clarity. Dashed lines denote the T_m of LLDPE1, HDPE1, and HDPE2 as guides to the eye. Arrows indicate the additional melting peaks other than those of the constituent materials.

Table 2. Thermal Properties of the PEs and Their Blends Calculated from DSC Thermograms (Figure 1)

sample	T_m (°C)	ΔH_m (J/g)[a]	crystallinity (X_j; %)[b]	calculated crystallinity of blends (X; %)[c]
LLDPE1	112	80	27	
HDPE1	132	171	58	
HDPE2	132	179	61	
HDPE1 20 wt %	111/126	100	34	33
HDPE2 10 wt %	111/119	98	33	30
HDPE2 20 wt %	112/125	110	37	34

[a]Enthalpy of fusion. [b]ΔH_m divided by ΔH_m° of 100% crystalline PE (293.6 J/g).[32] [c]$X = w_1X_1 + w_2X_2$, where w_j and X_j are the weight fraction and crystallinity of species *j*, respectively.

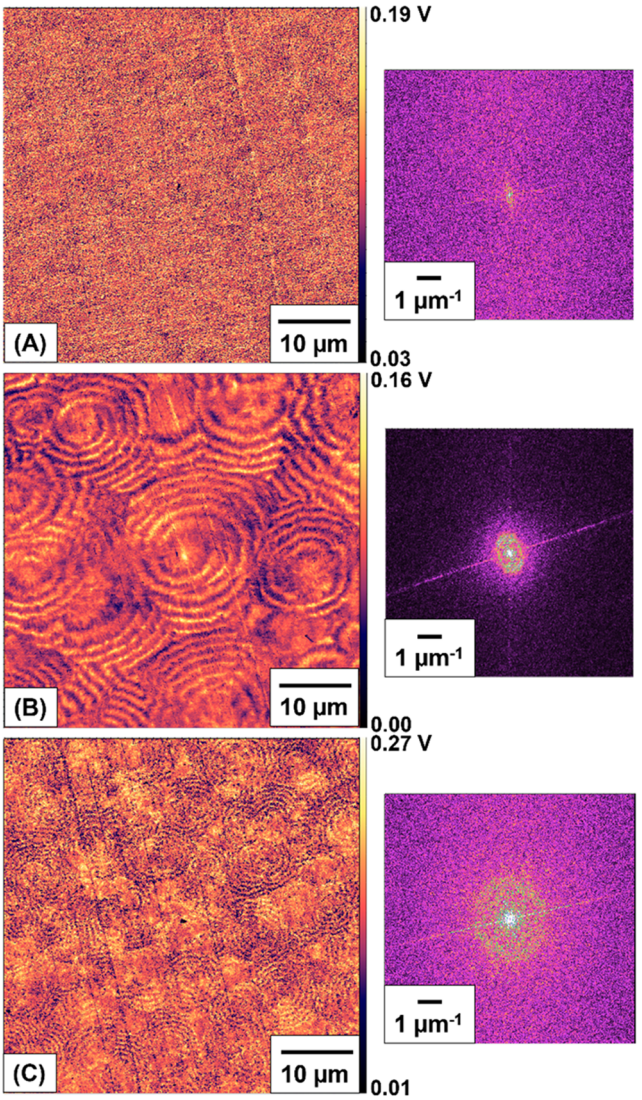

Figure 2. Representative IR absorbance images at 1472 cm^{-1} (left) for (A) LLDPE1, (B) HDPE2, and (C) HDPE2 20 wt %, and corresponding 2D Fourier transforms (FTs) (right). Image contrast scale limits are shown along the right edge of each image in units (volts) of raw transducer output; FT contrast scales are identical for panels (A−C).

https://doi.org/10.1021/acsapm.3c02211
ACS Appl. Polym. Mater. 2024, 6, 524−533

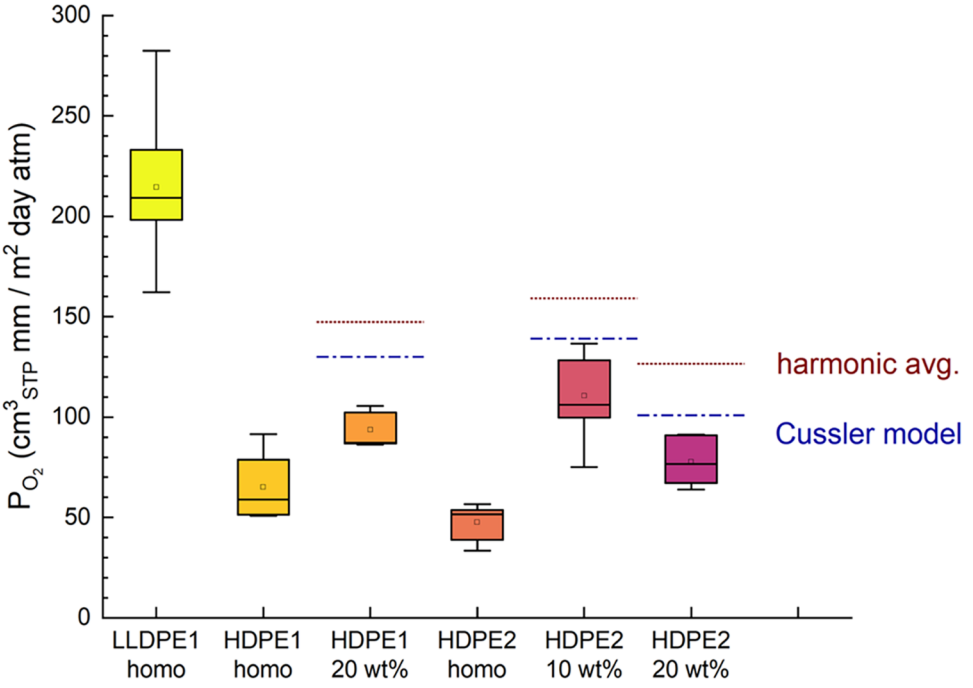

Figure 3. P_{O_2} of melt-pressed PE homopolymers and 10−20 wt % HDPE blended into the LLDPE1 matrix. Box plots indicate the median (solid line), mean (square symbol), and 25/75 quartiles; whiskers represent the total data range (minimum to maximum). Each box plot was obtained by measuring 4−10 samples. A lower P_{O_2} results in a higher oxygen barrier film. The dotted lines indicate the harmonic average P_{O_2} calculated by eq 1 using the mean P_{O_2} of the LLDPE1, HDPE1, and HDPE2 homopolymers (indicated by the square symbol on each box plot). The dashed−dotted lines indicate the P_{O_2} calculated using the Cussler model (eq 2 in the main text) using the same mean P_{O_2} of the homopolymers.

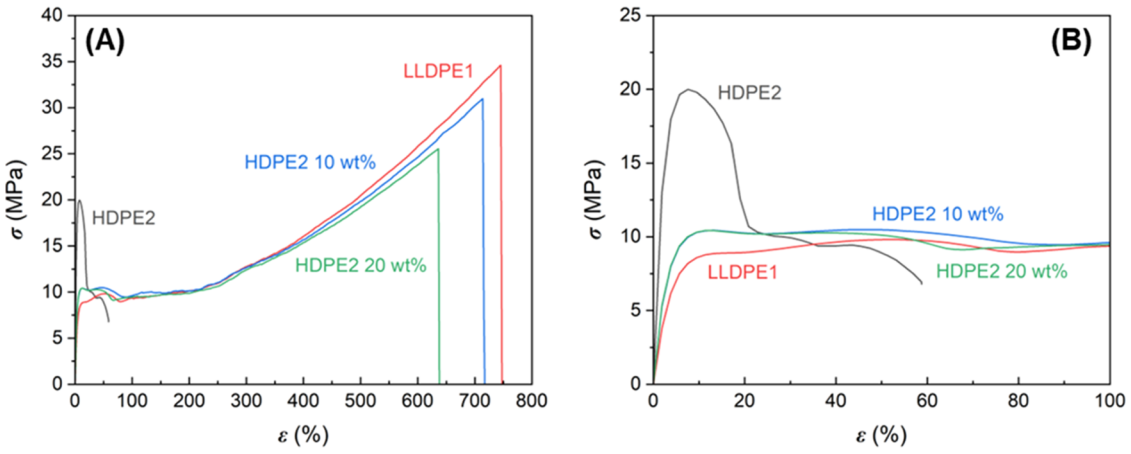

Figure 4. Uniaxial tensile responses of LLDPE1, HDPE2, and HDPE2 10−20 wt % blends. (A) Full profile; (B) magnified profile at low strain.

Table 3. Tensile Properties of LLDPE1, HDPE2, and Associated Blends; Extracted from the Uniaxial Tensile Responses (Figure 4)[a]

sample	E (MPa)	σ_y (MPa)	ε_y (%)	σ_b (MPa)	ε_b (%)
HDPE2	680 ± 1	20.2 ± 0.2	7.58 ± 0.01	5.0 ± 2.7	38 ± 6
LLDPE1	204 ± 5	8.75 ± 0.14	14.2 ± 0.3	34.3 ± 0.4	756 ± 11
HDPE2 10 wt %	253 ± 20	9.93 ± 0.6	13.0 ± 0.6	32.1 ± 1.0	727 ± 22
HDPE2 20 wt %	280 ± 3	10.4 ± 0.1	12.1 ± 0.2	25.6 ± 1.3	636 ± 24

[a]E: Young's modulus; σ_y: stress at yield; ε_y: elongation at yield; σ_b: stress at break; ε_b: elongation at break.

whereas the T_m of LLDPE1 was essentially unaffected by blending, which may have been caused by two contributing factors. As the HDPE and LLDPE are isomers having identical chemical formulas, the linear portions of the polymer chains from different grades of PEs may form crystals together.[29] Since HDPE starts to crystallize at a higher temperature than the LLDPE (Figure S1), the linear polymer chains of HDPE form crystal nuclei first and induce the crystallization (and potentially cocrystallization) of nearby LLDPE chains. At the same time, the presence of short branches of LLDPE may

https://doi.org/10.1021/acsapm.3c02211
ACS Appl. Polym. Mater. 2024, 6, 524−533

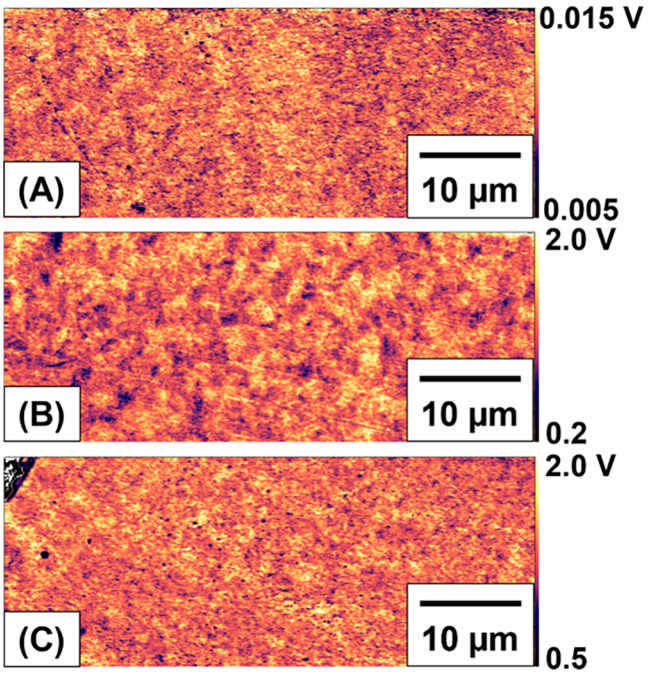

Figure 5. Representative IR absorbance images at the wavenumber of 1472 cm^{-1} for the blown films made of (A) LLDPE2, (B) HDPE2, and (C) LLDPE2/HDPE2 80/20 blend measured using AFM-IR. The data were obtained on cross sections of each film. (Because of significant variations in section thickness and thereby variations in IR absorbance, these images are presented following normalization to the simultaneously acquired height images; the latter scale zeroed to incorporate each measured section thickness.) Image contrast scale limits are shown along the right edge of each image in units (volts) of raw transducer output.

interfere with the chain folding of the linear chain portions, which could reduce the T_m of HDPE. Another possible factor that might have contributed to the lowering of HDPE T_m is the formation of thinner lamellar crystals in the blends, again likely caused by the presence of a short-branched LLDPE matrix. As lamellar thickness decreases, crystals become increasingly susceptible to melting due to the increasing surface energy contribution.[30]

The small peaks at ~118 °C for the HDPE1 20 wt % and HDPE2 10 wt % blends (indicated with arrows in Figure 1) also suggest some degree of cocrystallization since the peaks do not correspond to the melting of either pure component. The crystallinities of the blends are slightly larger than the calculated weighted average values (Table 2), which further indicates possible induced crystallization of LLDPE and cocrystallization of the two PE constituents. These observations collectively imply that HDPE likely induced enhanced crystallization of LLDPE1 at the interface. Note, however, that the chain folding during crystallization is far from equilibrium,[31] so the mechanism described here may not address the complete picture of what could be occurring in the systems of interest. Future studies on the details of crystallization kinetics may further reveal the physics underlying the crystallization of PE blends, which is not the main focus of this paper.

The microstructures of the melt-pressed films were further examined by using AFM-IR (Figure 2). The IR absorbance signal (amplitude of higher cantilever eigenmode resonance), manifested as a sharp peak at 1472 cm^{-1} in the full spectra, was chosen as a common gauge of PE crystallinity.[33] Mapping the IR amplitude at 1472 cm^{-1} enables clear visualization of crystalline lamellae in the samples without the ambiguity that may arise from uneven staining or electron charging when imaged with electron microscopic techniques. Representative IR absorbance images of LLDPE1 (such as Figure 2A) contain no spherulitic features, consistent with the low crystallinity measured by DSC. In contrast, images of HDPE2 clearly reveal spherulites as ripple-like patterns more than 10 μm in diameter (Figure 2B). The rippling morphology is further manifest as a high-intensity ring in the corresponding FT. Interestingly, similar images of the HDPE2 20 wt % blend also contain spherulite features similar to the HDPE2 homopolymer, albeit with smaller diameters (Figure 2C). The presence of a larger ring in the corresponding FT reflects the smaller distances between spherulitic ripples, compared to those in Figure 2B. The presence of smaller spherulites is consistent with the DSC result, which showed a reduced T_m of the HDPE2 in the blend film. Note that the bright central dots in the FTs (i.e., at very small inverse-space values) reflect large-scale positional displacements between entire spherulitic objects (confirmed via Fourier filtering and reverse-FT images, not shown), whereas the rings in the FTs reflect the spacing of bands within spherulites, which are coarser in Figure 2B. Linear features in the FTs derive from microtomy cutting marks seen as perpendicular lines in the IR absorbance images.

The contrast achieved in IR absorbance images was accompanied by less contrast in topography and conventional phase images, with the latter being sensitive mainly to the surface (Figure S2). Nevertheless, all such AFM image contrast is typically superior to what can be achieved using electron microscopy techniques via electronic spatial variations,[27] which should be minimal for polyethylene.

The stark contrast between the microstructures of LLDPE1 and the HDPE2 20 wt % blend is unexpected based on DSC as the crystallinity of the LLDPE1 increased only marginally more than expected from the weight fraction upon adding 20 wt % HDPE2. The result indicates that the addition of a small amount of HDPE caused LLDPE1 to form spherulites.

The formation of spherulites in LLDPE1 correlates with the recorded oxygen permeability of the films. Figure 3 shows the P_{O_2} of the melt-pressed PE homopolymers and the LLDPE/HDPE blends. Note that unlike the case for the OTR, P_{O_2} is independent of the film thickness, provided the internal structure does not change. In other words, any change in P_{O_2} would indicate a change in the film morphology. Measured P_{O_2} values of the PE homopolymers are within the range of those reported in the literature.[4] As anticipated, both HDPE1 and HDPE2 show lower P_{O_2} levels compared to pure LLDPE1 attributable to the high crystallinity of the added HDPE. However, blending a minor amount of either HDPE1 or HDPE2 into LLDPE1 leads to a greater reduction of P_{O_2} compared to the expected values calculated using common models that describe the reduction of the P_{O_2} of a matrix material upon adding low-permeability fillers.

First, we compared the experimental P_{O_2} of the blends to the harmonic average of the two constituent materials:[34,35]

$$\frac{1}{P_{O_2}} = \frac{\phi_1}{P_{O_{2,1}}} + \frac{\phi_2}{P_{O_{2,2}}} \quad (1)$$

https://doi.org/10.1021/acsapm.3c02211
ACS Appl. Polym. Mater. 2024, 6, 524−533

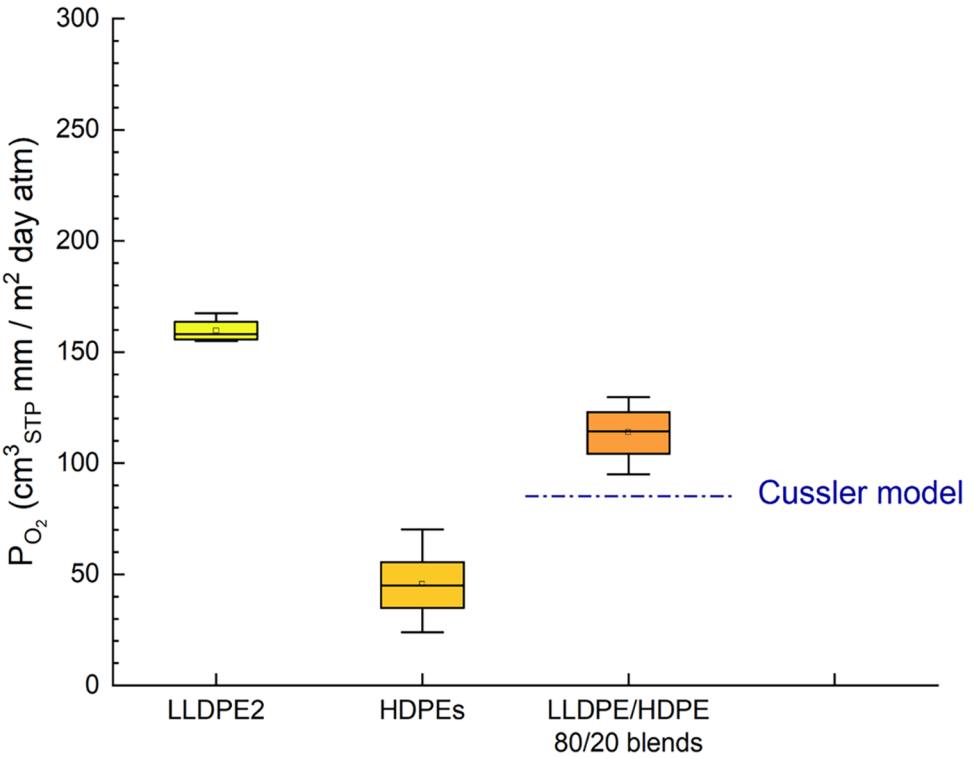

Figure 6. P_{O_2} of blown films made of LLDPE2, HDPE homopolymers, and blends containing 20 wt % HDPEs in the LLDPE2 matrix. Each box plot was obtained by measuring 3−5 sample specimens. The dashed−dotted lines indicate the P_{O_2} calculated by the Cussler model using the mean P_{O_2} of the homopolymers. Box plots indicate the median (solid line), mean (square symbol), and 25/75 quartiles; whiskers represent the total data range (minimum to maximum).

where $P_{O_2,j}$ and ϕ_j are the oxygen permeability coefficient and the volume fraction of component j, respectively. We used the mean value obtained from the experiment (i.e., represented by the square symbols in Figure 3) for $P_{O_2,j}$ to calculate the harmonic average values shown as dotted lines in Figure 3. P_{O_2} values of the LLDPE1/HDPE blends were ∼40% lower than the harmonic average. As the harmonic average model assumes a layer-by-layer stacking of the high- and low-permeability components within a film, the result indicates that the blended films showed gas barrier properties better than those of a layered film of the same LLDPE1/HDPE composition. We speculate that the collection of spherulites acted as multilayer-like barriers that generated tortuous pathways to retard the permeation of oxygen. The relatively small addition of highly crystalline HDPE may have induced the LLDPE1 matrix to change its morphology to enhance the oxygen blocking ability, evident from the formation of spherulites shown in Figure 2. If we assume that the added HDPEs have the same P_{O_2} as the corresponding HDPE homopolymers and the reduction of gas permeability is solely due to the morphological change of the LLDPE matrix, the "effective" P_{O_2} of LLDPE1 in the blends is calculated from eq 1to be 97−129 cm^3_{STP}·mm/(m^2·day·atm) compared to the measured value of 215 cm^3_{STP}·mm/(m^2·day·atm) for the LLDPE1 homopolymer. In other words, adding HDPEs induced reduction of the effective P_{O_2} of LLDPE by 40−55%.

As the spherulite microstructures in the films also resemble nanofiller-containing composites, we used a model that describes the permeability of filler-containing polymers suggested by Cussler and co-workers,[36] in which the system is portrayed as a film that contains disk-like fillers with zero permeability aligned in the film such that the long axis of the fillers is parallel to the film surface. According to this model, the P_{O_2} of a filler-containing polymer film is described by the following equation:

$$\frac{P_{O_2}}{P^{\circ}_{O_2}} = \frac{1-\phi}{1-\phi+\mu\alpha^2\phi^2} \tag{2}$$

where $P_{O_2}{}^{\circ}$ is the P_{O_2} of the matrix without fillers, ϕ is the volume fraction of fillers, μ is the geometry factor generally smaller than or equal to 1, and α is the aspect ratio of the fillers. The equation is valid when ϕ is small (<0.3) and $\alpha\phi > 1$ (i.e., large aspect ratio). In this work, we considered spherulites as the zero-permeability fillers and set the values $\mu = 1$ and $\alpha = 30$. According to the model, only the portions of spherulites in which the crystallites are aligned parallel to the film surface contribute to a significant reduction of P_{O_2}. Therefore, the shape of the effective fillers can be approximated as disks parallel to the surface, and the assumption of a large aspect ratio is valid. From geometrical consideration, the fraction of lamellar crystals in a single spherulite that is parallel to the film surface is $2/\pi \approx 64\%$ (Figure S3). Combining this calculated result with the crystallinity of the LLDPE1 and the blends yields $\phi = 0.17$ for LLDPE1, 0.22 for HDPE1 20 wt %, 0.21 for HDPE2 10 wt %, and 0.24 for HDPE2 20 wt %. Inserting the ϕ for LLDPE1 into eq 2, the hypothetical P_{O_2} of purely amorphous LLDPE1 matrix (i.e., 0% crystallinity) is calculated as $P^{\circ}_{O_2} = P_{O_2,\mathrm{LLDPE,amorphous}} = P_{O_2,\mathrm{LLDPE}}\cdot\left(\frac{1-\phi_{\mathrm{LLDPE}}}{1-\phi_{\mathrm{LLDPE}}+\mu\alpha^2\phi^2_{\mathrm{LLDPE}}}\right)^{-1} = 7100$

https://doi.org/10.1021/acsapm.3c02211
ACS Appl. Polym. Mater. 2024, 6, 524−533

cm^3_{STP}·mm/(m^2·day·atm). Using this value and ϕ for the blends, $P_{O_2,blend} = P_{O_2,LLDPE,amorphous} \cdot \frac{1-\phi_{blend}}{1-\phi_{blend}+\mu\alpha^2\phi^2_{blend}} = 130$ cm^3_{STP}·mm/(m^2·day·atm) for HDPE1 20 wt %, 139 cm^3_{STP}·mm/(m^2·day·atm) for HDPE2 10 wt %, and 101 cm^3_{STP}·mm/(m^2·day·atm) for HDPE2 20 wt %; the values are shown as the blue dashed−dotted lines in Figure 3. The experimentally observed P_{O_2} values of the blends are comparable to or smaller than the P_{O_2} calculated from this model as well; the reduction is the most significant in the HDPE1 20 wt % blend.

Interestingly, a significant reduction of P_{O_2} was observed for blends at the relatively low HDPE content of 10−20 wt %. This reduction of permeability is comparable to or better than our previous work, where we prepared many thin, alternating layers of LLDPE1 and isotactic polypropylene (Supporting Information). Isotactic polypropylene is highly crystalline, like HDPE, and thus can serve as a low-permeability additive. The 640-layer films of LLDPE1/PP (1:1 volume ratio) did not exhibit improved barrier properties over that of the bulk material, whereas the nominal 2560-layer films of LLDPE1/PP (8:2 volume ratio) showed reduced P_{O_2} compared to the harmonic average estimation (Figure S4). Since the PP layers in the 2560-layer film are considerably thinner than those in the 640-layer films, the reduction of P_{O_2} implies that the internal morphology and the resulting barrier properties of the PP layers have changed, potentially due to the confinement of PP in thin layers. If we assume that P_{O_2} of the LLDPE1 is the same as the bulk material and the reduction of P_{O_2} solely originated from the PP layer, the effective P_{O_2} of the confined PP calculated using eq 1 is 32.3 cm^3_{STP}·mm/(m^2·day·atm), compared to the mean value of the bulk PP, 75.7 cm^3_{STP}·mm/(m^2·day·atm) (Figure S4). The resulting 57% reduction of the effective P_{O_2} of PP in thin multilayers by confinement is comparable to the reduction observed in previous studies by Baer and co-workers[8,37] but not significantly better.

Although the materials used in this study are not considered high oxygen barriers by the industrial rule of thumb,[38,39] the better-than-expected improvement of oxygen barrier properties of LLDPE/HDPE blends suggests that the blending strategy in this work can be advantageous in producing improved packaging materials: blending requires much simpler instrumentation compared to multilayer extrusion, and the resulting films are readily recyclable as the constituents are all PE.

To examine the influence of crystalline HDPE on the mechanical properties of LLDPE, uniaxial tensile tests were performed. As shown in Figure 4 and Table 3, the LLDPE1 homopolymer had a lower elastic modulus but a much higher stress and elongation at break than the HDPE2 homopolymer. Adding 10−20 wt % of the relatively brittle HDPE2 to the LLDPE1 matrix led to a 24−37% increase in the elastic modulus, a 13−19% increase in the yield stress, a 7−25% decrease in the stress at break, and a 4−16% decrease in elongation at break. Considering the tensile test with oxygen barrier performance, adding ∼20 wt % HDPE would be optimal to enhance the oxygen barrier performance of LLDPE while retaining the beneficial mechanical properties.

In addition, the optical properties of the melt-pressed LLDPE1/HDPE films were compared with those of the LLDPE1 film (Figure S5). The blend films were indistinguishable from the LLDPE1 upon visual inspection. Adding 10−20 wt % HDPE did not significantly alter the appearance of the LLDPE1 film, which is beneficial for packaging applications.

The microstructure and oxygen barrier improvement of melt-pressed PE blend films were compared to those of blown films. We chose LLDPE and HDPE materials with melt flow indices better suited for film blowing than those used for melt pressing. LLDPE2 is estimated to have about twice the M_w of the LLDPE1 based on melt flow index. Evident in the representative AFM-IR images in Figure 5, the blown films of the PE homopolymers and blends lacked a spherulite morphology. The HDPE2 film image exhibited greater contrast (Figure 5B) than did the LLDPE2 film image (Figure 5A), which is suggestive of clustered crystalline domains, but a spherulite morphology with feature sizes as large as the case of melt-pressed samples was not observed (and FTs supported the real-space observations; data not shown). Images of LLDPE2 and its blend with HDPE2 also did not show a spherulite morphology. The blown films prepared with LLDPE2/HDPE blends showed somewhat increased haze compared to the LLDPE2 blown film due to the inclusion of highly crystalline HDPE but a negligible decrease in optical transmittance (Table S1).

The DSC traces of the blown films made of LLDPE2, HDPE5, and HDPE5 20 wt % blend are shown in Figure S6 and Table S2; blends of LLDPE2 with the other HDPEs showed similar behavior. The T_m of LLDPE2 and HDPE5 in the blend decreased by ∼3 and ∼12 °C, respectively, compared to those of the corresponding homopolymers. Overall, the DSC results of blown films were not noticeably different from those of melt-pressed films other than somewhat higher crystallinities of the constituent PEs, despite the large melt flow index differences between the LLDPE1 vs LLDPE2 and HDPE1 vs HDPE5.

The P_{O_2} values of blown films of LLDPE2, HDPEs, and blends are shown in Figure 6. As the P_{O_2} values of HDPE1, 3, 4, and 5 (and those of the 20 wt % blends made with different HDPE) were close to each other, the results from different HDPEs were consolidated to single box plots (the second and third entries in Figure 6). All tested blown films made of LLDPE2/HDPE blends containing 20 wt % HDPEs showed P_{O_2} values larger than what is expected from the nanofiller model by Cussler and co-workers.[36] The lack of a spherulite morphology and the resulting absence of tortuous pathways for gas molecules are reflected in the oxygen barrier properties of the blown films. Our blown films were manufactured at a drawdown ratio of ∼10 and a blow-up ratio of 2.5. These experimental conditions lead to shish−kebab-type crystal formation as the polyethylene rapidly cools and crystallizes. Long chains orient in the machine direction to form a "shish" (i.e., the stem part from which multiple spherulite crystals may start to grow), while shorter chains form spherulite "kebabs" whose disk-like cross sections tend to orient perpendicular to the film surface.[23,40] The higher M_w of LLDPE2 compared to that of LLDPE1 will likely lead to more shish formation. This perpendicular orientation of the spherulite lamellae is more permeable than the parallel orientation, thus increasing the permeability in blown film samples. In contrast, the compression molded samples cool slowly, giving polyethylene chains time to form spherulites with a greater percentage of lamella oriented parallel with respect to the sample surface. This will decrease permeability and allow for spherulite detection using techniques such as AFM-IR as shown in

https://doi.org/10.1021/acsapm.3c02211
ACS Appl. Polym. Mater. 2024, 6, 524−533

Figure 2. Note that the blow-up ratio of 2.5 used in this study, although not far from commonly used values in the literature,[22,23] is lower than the typically used condition (~4.0) in industry. At a higher blow-up ratio, shear-induced crystallization along the extended chains would be more prominent, and the parallel alignment of shish with respect to the film surface would be more prevalent. Thus, using a blow-up ratio higher than 2.5 would not detract the argument made here.

CONCLUSIONS

This work demonstrated a greater than expected enhancement of the oxygen barrier properties of LLDPE by blending with HDPE and preparing films by melt pressing. The films of the LLDPE/HDPE blends reduced P_{O_2} levels greater than expected from the harmonic average model and zero-permeability nanofiller model. The reduction of P_{O_2} is attributed to the promotion of spherulite formation by HDPE in the LLDPE matrix, resulting in tortuous pathways for the diffusion of oxygen molecules. If we assume that the reduction of permeability is solely from the morphological change of LLDPE induced by adding HDPEs, then the LLDPE matrix in the blends was calculated to have 40−55% smaller effective P_{O_2} compared to the LLDPE homopolymer. For the first time, we find significant formation of spherulites in the LLDPE matrix, evidenced by AFM-IR images, even at 10% addition of HDPE. We also demonstrated the role of processing in controlling permeability. The results from melt-pressed films contrast with similar compositions prepared by film blowing, which did not show barrier enhancement beyond expectation. AFM-IR showed that the blown films lacked spherulite crystals likely due to stretching in the machine direction followed by rapid cooling. Although the materials developed in this study are not high-barrier materials based on industrial standards, further improvement of the barrier performance could result in easily recyclable LLDPE-based packaging materials without the need for additives to achieve high barrier properties. It would be interesting to explore how sheet extrusion or blow molding processes influence the permeability of blends of HDPE and LLDPE.

ASSOCIATED CONTENT

Supporting Information

The Supporting Information is available free of charge at https://pubs.acs.org/doi/10.1021/acsapm.3c02211.

DSC crystallization traces of melt-pressed films, AFM topography and phase data of HDPE1, calculation of the fraction of lamellar crystals in a single spherulite that is perpendicular to the film surface, preparation and P_{O_2} measurement of LLDPE1/polypropylene multilayer films, optical characteristics of LLDPE and LLDPE/HDPE blend films, and DSC of the blown films made of LLDPE2, HDPE5, and HDPE5 20 wt % blend (PDF)

AUTHOR INFORMATION

Corresponding Author

Kyungtae Kim − *Department of Chemical Engineering and Materials Science, University of Minnesota, Minneapolis, Minnesota 55455, United States; Materials Physics and Applications Division, Center for Integrated Nanotechnologies, Los Alamos National Laboratory, Los Alamos, New Mexico 87545, United States;* orcid.org/0000-0002-3206-8494; Email: kyungtae@lanl.gov

Authors

Aristotle J. Zervoudakis − *Department of Chemical Engineering and Materials Science, University of Minnesota, Minneapolis, Minnesota 55455, United States;* orcid.org/0000-0002-4758-1784

Jacob A. LaNasa − *Materials Physics and Applications Division, Center for Integrated Nanotechnologies, Los Alamos National Laboratory, Los Alamos, New Mexico 87545, United States;* Present Address: Engineered Materials Group (MST-7), Materials Science and Technology Division, Los Alamos National Laboratory, Los Alamos, New Mexico 87545, United States

Greg Haugstad − *Characterization Facility, University of Minnesota, Minneapolis, Minnesota 55455, United States*

Fang Zhou − *Characterization Facility, University of Minnesota, Minneapolis, Minnesota 55455, United States;* orcid.org/0000-0001-9442-6288

Bongjoon Lee − *Department of Chemical Engineering and Materials Science, University of Minnesota, Minneapolis, Minnesota 55455, United States*

Olivier Lhost − *TotalEnergies OneTech Belgium, Seneffe 7181, Belgium*

Yves Trolez − *TotalEnergies OneTech Belgium, Seneffe 7181, Belgium*

Frank S. Bates − *Department of Chemical Engineering and Materials Science, University of Minnesota, Minneapolis, Minnesota 55455, United States;* orcid.org/0000-0003-3977-1278

Christopher W. Macosko − *Department of Chemical Engineering and Materials Science, University of Minnesota, Minneapolis, Minnesota 55455, United States;* orcid.org/0000-0002-2892-3267

Complete contact information is available at: https://pubs.acs.org/10.1021/acsapm.3c02211

Author Contributions

K.K., O.L., F.S.B., and C.W.M. conceived the research; K.K., A.J.Z., J.A.L., G.H., F.Z., and B.L. performed experiments; K.K., A.J.Z., J.A.L., G.H., O.L., Y.T., and C.W.M. analyzed the data; and K.K., A.J.Z., J.A.L., G.H., F.Z., and C.W.M. wrote the manuscript with comments and input from all authors.

Notes

The authors declare no competing financial interest.

ACKNOWLEDGMENTS

This research was funded by TotalEnergies. The authors thank Dr. Christopher Thurber at the Dow Chemical Company for helpful discussions and for providing the HDPE2 sample. G.H. acknowledges financial support from the University of Minnesota Industrial Partnership for Research in Interfacial and Materials Engineering (IPRIME) program. Parts of this research were carried out at the Characterization Facility, University of Minnesota, which receives partial support from the National Science Foundation (NSF) through the MRSEC (Award Number DMR-2011401) and the NNCI (Award Number ECCS-2025124) programs. Parts were performed at the Center for Integrated Nanotechnologies (CINT), an Office of Science User Facility operated for the U.S. Department of Energy (DOE) Office of Science. Los Alamos National

Laboratory, an affirmative action equal opportunity employer, is managed by Triad National Security, LLC for the U.S. DOE's NNSA, under Contract 89233218CNA000001.

REFERENCES

(1) Verified Market Research. *Global Polyethylene Packaging Market Size by Product [High Density Polyethylene (HDPE), Low Density Polyethylene (LDPE), and Linear Low Density Polyethylene (LLDPE)], by Application (Food, Drinks, Electronic Products), by Geographic Scope and Forecast*; Verified Market Research: Lewes, DE, 2022.
(2) Transparency Market Research. *LLDPE Films Market-Global Industry Analysis, Size, Share, Growth, Trend and Forecast 2018−2028*; Transparency Market Research: Albany, NY, 2022.
(3) An, M.; Cui, B.; Duan, X. Preparation and applications of linear low-density polyethylene. *J. Phys. Conf. Ser.* **2022**, *2229*, No. 012009.
(4) Butler, T. I.; Morris, B. A. PE-Based Multilayer Film Structures. In *Multilayer Flexible Packaging*, 2nd ed.; Wagner, J. R., Jr., Ed.; William Andrew Publishing: Oxford, UK, 2016; pp 281−310.
(5) Videira-Quintela, D.; Martin, O.; Montalvo, G. Recent advances in polymer-metallic composites for food packaging applications. *Trends Food Sci. Technol.* **2021**, *109*, 230−244.
(6) Zhang, T.; Yu, Q.; Fang, L.; Wang, J.; Wu, T.; Song, P. All-organic multilayer coatings for advanced poly(lactic acid) films with high oxygen barrier and excellent antifogging properties. *ACS Appl. Polym. Mater.* **2019**, *1*, 3470−3476.
(7) Merritt, S. M. J.; Wemyss, A. M.; Farris, S.; Patole, S.; Patias, G.; Haddleton, D. M.; Shollock, B.; Wan, C. Gas barrier polymer nanocomposite films prepared by graphene oxide encapsulated polystyrene microparticles. *ACS Appl. Polym. Mater.* **2020**, *2*, 725−731.
(8) Huang, H.-D.; Ren, P.-G.; Zhong, G.-J.; Olah, A.; Li, Z.-M.; Baer, E.; Zhu, L. Promising strategies and new opportunities for high barrier polymer packaging films. *Prog. Polym. Sci.* **2023**, *144*, No. 101722.
(9) Dingwell, C. E.; Hillmyer, M. A. Regiospecific poly(ethylene-co-vinyl alcohol) by ROMP of 3-acetoxycyclooctene and postpolymerization modification for barrier material applications. *ACS Appl. Polym. Mater.* **2023**, *5*, 1828−1836.
(10) PE Flexible Films Recycling: New Findings for Functional Barriers, 2023. https://recyclass.eu/news/pe-flexible-films-recycling-new-findings-for-functional-barriers/.
(11) Dow Chemical Company Recycle Ready Technology from Dow Receives Recyclass Recyclability, 2023. https://www.packworld.com/supplier-news/news/22847355/dow-chemical-company-recycleready-technology-from-dow-receives-recyclass-recyclability-approval.
(12) Wang, J.; Gardner, D. J.; Stark, N. M.; Bousfield, D. W.; Tajvidi, M.; Cai, Z. Moisture and oxygen barrier properties of cellulose nanomaterial-based films. *ACS Sustainable Chem. Eng.* **2018**, *6*, 49−70.
(13) Wang, H.-S.; Chen, D.; Chuai, C.-Z. Mechanical and barrier properties of LLDPE/chitosan blown films for packaging. *Packag. Technol. Sci.* **2015**, *28*, 915−923.
(14) Shields, R. J.; Bhattacharyya, D.; Fakirov, S. Microfibril-reinforced composites from PE/PET blends: effect of reinforcement size on oxygen permeability. *Key Eng. Mater.* **2007**, *334−335*, 249−252.
(15) Tan, S. N. S.; Somashekar, A. A.; Bhattacharyya, D. Development and analysis of gas barrier properties of microfibrillar polymer−polymer composites. *J. Mater. Sci.* **2015**, *50*, 7384−7397.
(16) Arunvisut, S.; Phummanee, S.; Somwangthanaroj, A. Effect of clay on mechanical and gas barrier properties of blown film LDPE/clay nanocomposites. *J. Appl. Polym. Sci.* **2007**, *106*, 2210−2217.
(17) Kuila, T.; Bose, S.; Mishra, A. K.; Khanra, P.; Kim, N. H.; Lee, J. H. Effect of functionalized graphene on the physical properties of linear low density polyethylene nanocomposites. *Polym. Test.* **2012**, *31*, 31−38.
(18) Silva-Leyton, R.; Quijada, R.; Bastías, R.; Zamora, N.; Olate-Moya, F.; Palza, H. Polyethylene/graphene oxide composites toward multifunctional active packaging films. *Compos. Sci. Technol.* **2019**, *184*, No. 107888.
(19) Huang, H.-D.; Zhou, S.-Y.; Zhou, D.; Ren, P.-G.; Xu, J.-Z.; Ji, X.; Li, Z.-M. Highly efficient "composite barrier wall" consisting of concentrated graphene oxide nanosheets and impermeable crystalline structure for poly(lactic acid) nanocomposite films. *Ind. Eng. Chem. Res.* **2016**, *55*, 9544−9554.
(20) Jordan, A. M.; Meyer, L.; Kim, K.; Lee, B.; Bates, F. S.; Macosko, C. W. Improved polypropylene thermoformability through polyethylene layering. *ACS Appl. Mater. Interfaces* **2022**, *14*, 34134−34142.
(21) Jordan, A. M.; Kim, K.; Soetrisno, D.; Hannah, J.; Bates, F. S.; Jaffer, S. A.; Lhost, O.; Macosko, C. W. Role of crystallization on polyolefin interfaces: An improved outlook for polyolefin blends. *Macromolecules* **2018**, *51*, 2506−2516.
(22) Morris, B. A. The effect of coextrusion on bubble kinematics, temperature distribution and property development in the blown film process. *J. Plast. Film Sheeting* **1999**, *15*, 25−36.
(23) Chatterjee, T.; Patel, R.; Garnett, J., IV; Paradkar, R.; Ge, S.; Liu, L.; Forziati, K. T., Jr.; Shah, N. Machine direction orientation of high density polyethylene (HDPE): Barrier and optical properties. *Polymer* **2014**, *55*, 4102−4115.
(24) ASTM D3985-17 *Standard Test Method for Oxygen Gas Transmission Rate Through Plastic Film and Sheeting Using a Coulometric Sensor*; ASTM, 1998.
(25) ASTM D1434-23 *Standard Test Method for Determining Gas Permeability Characteristics of Plastic Film and Sheeting*; ASTM, 1998.
(26) Mathurin, J.; Deniset-Besseau, A.; Bazin, D.; Dartols, E.; Wagner, M.; Dazzi, A. Photothermal AFM-IR spectroscopy and imaging: Status, challenges, and trends. *J. Appl. Phys.* **2022**, *131*, No. 010901.
(27) Tri, P. N.; Prud'homme, R. E. Nanoscale lamellar assembly and segregation mechanism of poly(3-hydroxybutyrate)/poly(ethylene glycol) blends. *Macromolecules* **2018**, *51*, 181−188.
(28) Haugstad, G. *Atomic Force Microscopy: Understanding Basic Modes and Advanced Applications*; John Wiley & Sons, Inc.: Hoboken, NJ, 2012.
(29) Niaounakis, M.; Kontou, E. Effect of LDPE on the thermomechanical properties of LLDPE-based films. *J. Polym. Sci., Part B: Polym. Phys.* **2005**, *43*, 1712−1727.
(30) Höhne, G. W. H. Another approach to the Gibbs-Thompson equation and the melting point of polymers and oligomers. *Polymer* **2002**, *43*, 4689−4698.
(31) Lotz, B.; Miyoshi, T.; Cheng, S. Z. D. 50th Anniversary perspective: Polymer crystals and crystallization: Personal journeys in a challenging research field. *Macromolecules* **2017**, *50*, 5995−6025.
(32) Wunderlich, B.; Cormier, C. M. Heat of fusion of polyethylene. *J. Polym. Sci., Part A: Polym. Chem.* **1967**, *5*, 987−988.
(33) Smith, B. C. *Infrared Spectral Interpretation: A Systematic Approach*; CRC Press: Boca Raton, FL, 1999.
(34) Kolařík, J.; Fambri, L.; Pegoretti, A.; Penati, A. Prediction of the gas permeability of heterogeneous polymer blends. *Polym. Eng. Sci.* **2000**, *40*, 127−131.
(35) Su, H.; Xue, J.; Cai, P.; Li, J.; Guo, S. Structure and oxygen-barrier properties of (linear low-density polyethylene/ethylene-vinyl alcohol copolymer)/linear low-density polyethylene composite films prepared by microlayer coextrusion. *J. Appl. Polym. Sci.* **2015**, *132*, 42211.
(36) DeRocher, J.; Gettelfinger, B.; Wang, J.; Nuxoll, E.; Cussler, E. Barrier membranes with different sizes of aligned flakes. *J. Membr. Sci.* **2005**, *254*, 21−30.
(37) Zhang, G.; Lee, P. C.; Jenkins, S.; Dooley, J.; Baer, E. The effect of confined spherulite morphology of high-density polyethylene and polypropylene on their gas barrier properties in multilayered film systems. *Polymer* **2014**, *55*, 4521−4530.
(38) Oxygen Transmission Rate, 2023. https://www.polyprint.com/understanding-film-properties/flexographic-otr/.

https://doi.org/10.1021/acsapm.3c02211
ACS Appl. Polym. Mater. 2024, 6, 524−533

(39) Understanding OTR & MVTR Specifications for Barrier Food Packaging, 2023. https://blog.icpg.co/understanding-otr-mvtr-specifications-for-barrier-food-packaging.
(40) Somani, R. H.; Yang, L.; Zhu, L.; Hsiao, B. S. Flow-induced shish-kebab precursor structures in entangled polymer melts. *Polymer* **2005**, *46*, 8587−8623.

https://doi.org/10.1021/acsapm.3c02211
ACS Appl. Polym. Mater. 2024, 6, 524−533